ELSEVIER

CrossMark

Chinese Astronomy and Astrophysics 49-3 (2025) 565–578

CHINESE
ASTRONOMY
AND ASTROPHYSICS

Research on the Analysis Method of Asteroid Impact Probability† ⋆

ZHENG Hang[1,2] ZHU Qing-feng[1,2,3△] SONG Ye-zhi[4△△] LI Xu-zhi[1,2]
XU Xiao-hui[1,2] QIU Jin-sheng[1,2] ZHAO Jun-han[1,2]

[1] *CAS Key Laboratory for Research in Galaxies and Cosmology, Department of Astronomy, University of Science and Technology of China, Hefei 230026*

[2] *School of Astronomy and Space Sciences, University of Science and Technology of China, Hefei 230026*

[3] *Deep Space Exploration Laboratory, Hefei 230088*

[4] *Shanghai Astronomical Observatory, Chinese Academy of Sciences, Shanghai 200030*

Abstract In view of the current situation of inconsistent conclusions among existing asteroid impact monitoring systems, the linear approximation method used in the change line impact monitoring system was studied, and the conclusion is achieved that the deviation of the orbit distribution relative to the theoretical orbit distribution obtained by this method gradually became significant as the orbit propagation time increased. The impact probability of 6 asteroid instances was calculated using the Monte Carlo method. Compared with the results of the existing Monte Carlo impact monitoring system, the maximum difference is 2.1 times the standard deviation. The impact samples of asteroid 2020 VV in October 2056 are analyzed in detail, and the distribution of impact samples with time and space is depicted, and the conclusions are consistent with those of existing impact monitoring systems. As for the comparison between the different impact monitoring systems, it is concluded that the Monte Carlo impact monitoring system and the change line impact monitoring system currently have their own advantages and disadvantages: the former does not introduce the error caused by the linear approximation method, but the computational cost is high. The linear approximation method used in the latter will bring errors, but it can

† Supported by the Strategic Priority Research Program of the Chinese Academy of Sciences (Grant No. XDB 41000000)

Received 2024-05-06; revised version 2024-08-02

⋆ A translation of *Acta Astron. Sin.* Vol. 66, No. 3, pp. 29.1–29.9, 2025

△ zhuqf@ustc.edu.cn

△△ syz@shao.ac.cn

PII:
10.1016/j.chinastron.2025.09.010

find some virtual impact sources with low impact probability that may be missed by the former, and the computational cost is relatively low.

Key words minor planets, asteroids: near-Earth asteroids impact monitoring, astrometry and celestial mechanics, methods: data analysis

1. INTRODUCTION

Currently, there are multiple analysis methods for near-earth object (NEO) impact monitoring (IM)[1]. In 1999, the CLOMON impact monitoring system operated by the University of Pisa introduced the use of a one-dimensional space along the maximal stretching direction of confidence region (CR), known as the line of variations (LOV)[2], for impact probability analysis. Compared to the first-generation CLOMON, the subsequent CLOMON2 employs an updated astrometric error model[3]. NASA's Jet Propulsion Laboratory (JPL) employs the same analysis method as CLOMON[4] in its Sentry system for impact probability computation. Sentry-II implements upgrades by adopting the Monte Carlo (MC) method to sample within the six-dimensional orbital parameter space. In order to obtain high-precision results under acceptable computational resource consumption, Sentry-II employs the importance sampling technique to preferentially sample the regions of the orbital parameter space with high impact probability[5]. Furthermore, the Asteroid Orbit Determination (AstOD) system, developed by SpaceDyS for ESA's Near-Earth Object Coordination Centre (NEOCC), employs algorithms similar to CLOMON2, but features a distinct computational engine[6] adaptable to different operating systems. All three asteroid impact monitoring systems utilize observational data collected by the Minor Planet Center (MPC) for impact monitoring and analysis. The alerts generated by CLOMON2, Sentry-II, and AstOD are respectively published on NEODyS, the Center for NEO Studies (CNEOS), and NEOCC platforms. In subsequent discussions, these impact monitoring systems will be referred to by their corresponding publication platform names.

Conventional impact monitoring operates on timescales of approximately 100 years, as prolonged orbit propagation leads to excessive orbit dispersion that compromises prediction accuracy. Fuentes-Munoz et al.[7] pioneered a method for assessing asteroid impact risks across millennial timescales. Conventional impact monitoring systems target the objects with relatively sufficient observational data, enabling high-precision orbit determination through the least squares (LS) method. The derived orbital solutions can characterize the orbit distribution of asteroids, thereby facilitating their impact probability analysis. If the observational data of objects is limited (e.g., with an observation arc shorter than 1°), high-precision orbit determination and distribution become unattainable, necessitating variation of the analysis method. When orbit determination converges through the LS method, where the orbit distribution's CR exhibits a two-dimensional disk-like characteristic, and cannot be represented by an LOV, two-dimensional LOV (2D-LOV) processing becomes necessary[8]. Conversely, when LS orbit determination fails to converge, the orbit distribution can be

analyzed using the admissible region (AR)[9] approach. The impact monitoring systems for such special cases include: JPL's Scout system[10] (with relevant data published on CNEOS), the University of Pisa's NEOScan system[11] (with relevant data published on NEODyS), and the University of Helsinki's NEORANGER system[12].

Differences exist in the computation results of impact probability among conventional impact monitoring systems: The top three objects with the highest cumulative impact probabilities in CNEOS were not included in NEOCC's warning list, while computed impact probabilities differed for objects receiving concurrent alerts from both systems (as of April 15, 2024). In view of this situation, this paper analyzes the errors introduced by the LOV impact monitoring system, and computes the impact probabilities of some asteroid instances using the MC method, thereby validating the results of existing impact monitoring systems. This paper is organized as follows: Section 2 presents the computation method of asteroid impact probability employed in this study and its uncertainty analysis; Section 3 analyzes the errors introduced by the linear approximation method used in the LOV impact monitoring system; Section 4 computes the impact probabilities of some asteroid instances using the MC method, and analyzes the impact samples of asteroid 2020 VV in October 2056 in detail; Section 5 provides a comprehensive summary of the entire paper.

2. IMPACT PROBABILITY COMPUTATION METHOD

High-risk asteroids may reach perilously close distances to Earth, a condition designated as a close approach (CA), where the internationally recognized distance threshold for CA is 0.05 AU. During the CA, it is necessary to establish an appropriate reference frame to study the asteroid-Earth relationship, typically by constructing the reference frame and its coordinate system based on the target plane (TP)[13].

2.1 Target Plane

TP is a geocentric plane passing through Earth's center, with the TP coordinate system having its origin at the geocenter. The normal direction of the TP is parallel to the asteroid's geocentric velocity. More precisely, there are two definitions of the TP: The first type is designated as the TP or B-plane, which is perpendicular to the direction of the asteroid's geocentric unperturbed relative velocity at infinity (V_∞) (here, "infinity" refers to a position outside Earth's sphere of gravitational influence, where CA is considered to have already closely occurred); The second type is designated as the Modified Target Plane (MTP), which is perpendicular to the direction of the asteroid's velocity at its closest approach to Earth ($V_{\rm CA}$). As illustrated in Fig. 1, CA represents the point of minimum geocentric distance along the asteroid's trajectory. Both the B-plane and the MTP pass through Earth's center, with the B-plane perpendicular to V_∞ and the MTP perpendicular to $V_{\rm CA}$. The two types of target planes differ fundamentally in their representation of gravitational effects: On the MTP, the asteroid's deflection caused by Earth's gravitational perturbation is directly

visible, since the intersection point of the asteroid's trajectory with the MTP marks its closest approach position; in contrast, the B-plane inherently obscures gravitational influence information. For CA events with higher relative velocities or at larger geocentric distances, the asteroid's orbit deflection becomes insignificant, rendering the distinction between the two types of target planes negligible. The subsequent discussions will employ the MTP for asteroid impact analysis.

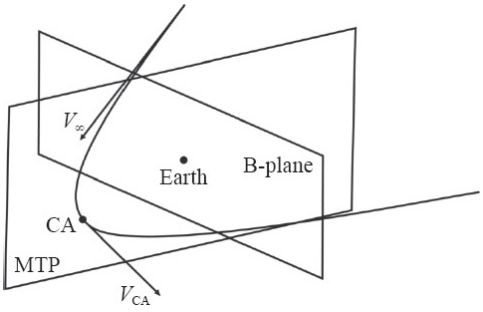

Fig. 1 Geometric figure of target plane.

2.2 Orbit Distribution and Confidence Region

Asteroid orbits are determined through the computation of observational data. Observational data inherently contains uncertainties, which consequently introduces uncertainties in the determination of asteroid orbits. These orbital uncertainties can be estimated using a Gaussian distribution model[4]. The nominal orbital solution is denoted as X^*, then this Gaussian distribution takes X^* as the mean value, and Γ (the covariance matrix of orbit determination) as the covariance matrix:

$$q(\boldsymbol{X}) \sim N\left(\boldsymbol{X}^*, \boldsymbol{\Gamma}\right), \tag{1}$$

where q represents the probability density function (PDF), X denotes the orbital parameter, and N stands for the standard Gaussian (normal) distribution function. The CR (Confidence Region) in the orbital parameter space is determined by the variation of the objective function in LS orbit determination, and constitutes the orbital parameter search space for asteroid impact analysis. CR is defined as the parameter space where the variation of the objective function does not exceed a specified threshold:

$$\frac{\Delta \boldsymbol{X}^{\mathrm{T}} \boldsymbol{\Gamma}^{-1} \Delta \boldsymbol{X}}{m} < \frac{\chi^2}{m}, \tag{2}$$

where m denotes the number of observation points, ΔX represents the deviation of the orbital parameter vector from the nominal solution, and χ^2 stands for a user-defined parameter that constrains the CR size.

2.3 Monte Carlo Method

The dynamical model of asteroids involves the N-body problem, making their orbits analytically intractable. It is impossible to directly obtain all future orbit states within the CR through analytical methods. Only by employing numerical integration can a finite number of orbit states sampled from the CR be analyzed. Consequently, the MC method can be employed to analyze asteroid impact probability[14].

As described above, when observational data is relatively sufficient, the nominal orbital solutions of asteroids can be obtained through LS orbit determination, thereby enabling the determination of their orbit distributions. The region in the orbital parameter space where impacts may occur is denoted as F. The region F is also referred to as the Virtual Impactor (VI), defined as a subset of the orbital parameter space where impacts may occur[6]. The impact probability is given by:

$$P_{\text{Impact}} = \int_F q(\boldsymbol{X})\mathrm{d}\boldsymbol{X}, \tag{3}$$

where P_{Impact} provides the exact representation of impact probability. Samples drawn from the CR are designated as Virtual Asteroids (VAs). Each sample is then dynamically propagated to assess its Earth-impact probability, equivalent to determining whether the corresponding VA sample resides within the region F. Through:

$$\hat{P}_{\text{Impact}} = \frac{N_{\text{VI}}}{N_{\text{VA}}}, \tag{4}$$

the estimated impact probability is derived. In Eq. (4), N_{VA} is the number of VAs, and N_{VI} is the number of VAs in VI. According to Reference[15], the MC sampling method employed in this study belongs to repeated sampling of random variables following a binomial distribution, where sample statistics are used to estimate the distribution parameters of the variables:

$$\begin{aligned} \hat{\mu} &= \bar{X} \equiv \frac{1}{n}\sum_{i=1}^{n} X_i, \\ \hat{\sigma}^2 &= \frac{1}{n-1}\sum_{i=1}^{n}\left(X_i - \bar{X}\right)^2, \end{aligned} \tag{5}$$

where $\hat{\mu}$ and $\hat{\sigma}$ stands for the unbiased estimators of the variable's expectation and standard deviation, respectively, n is the sample size, X_i denotes the sample, and $\bar{X}$ represents the sample mean. For this study, X_i is assigned a value of 1 for impact samples and 0 for non-impact samples. With such notational conventions, the estimated impact probability can also be expressed as:

$$\hat{P}_{\text{Impact}} = \bar{X}. \tag{6}$$

According to the description of the Central Limit Theorem (CLT) in Reference[15], the distribution of the mean $\bar{X}$ with independent and identically distributed variables asymptotically approaches a Gaussian distribution as the sample size increases:

$$\lim_{n\to\infty}\left(\frac{\bar{X}-\mu}{\sqrt{\frac{\sigma^2}{n}}}\leqslant x\right)=\Phi(x), \tag{7}$$

where μ and σ stand for the variable's expectation and standard deviation, respectively, and $\Phi(x)$ represents the standard Gaussian cumulative distribution function. Substituting the estimates of $\hat{\mu}$ and $\hat{\sigma}$ from Eq. (5) into Eq. (7) yields an estimate of the standard deviation $\sqrt{\frac{\sigma^2}{n}}$ of the Gaussian distribution approached by the sample mean $\bar{X}$, which also serves as an estimate of the uncertainty of the sample mean $\bar{X}$:

$$\hat{\sigma}_{\hat{P}_{\mathrm{Impact}}}=\hat{\sigma}_{\bar{X}}=\sqrt{\frac{1}{n(n-1)}\sum_{i=1}^{n}\left(X_i-\bar{X}\right)^2}. \tag{8}$$

Eqs. (6) and (8) provide the expressions for estimating the asteroid impact probability and its uncertainty, respectively.

3. ERRORS IN THE LINE-OF-VARIATIONS (LOV) IMPACT MONITORING SYSTEM

The NEOCC and NEODyS impact monitoring systems employ the LOV method to analyze impact probability, which sample in the two-dimensional LOV space, evaluate the CA distances between LOV samples and Earth, and identify points of minimum CA distance to Earth along the LOV. Using the linear approximation method, the orbit distribution at the CA epoch is estimated for each local point of minimum CA distance[16] through transformation of the orbital covariance matrix to the orbital covariance matrix at the CA epoch:

$$\boldsymbol{\Gamma}(t)=\boldsymbol{\Phi}\boldsymbol{\Gamma}\left(t_0\right)\boldsymbol{\Phi}^{\mathrm{T}}, \tag{9}$$

where $\boldsymbol{\Phi}\equiv\frac{\partial\boldsymbol{X}(t)}{\partial\boldsymbol{X}(t_0)}$ denotes the state transition matrix[17, 18], t and t_0 represent the time variable and the initial time, respectively. According to the orbit distribution computation method described previously, the orbital covariance matrix at the CA epoch is taken as the orbit distribution parameter at that epoch. This yields the orbit distribution at the CA epoch, which is then used to establish a linear mapping between the asteroid's impact points on the TP and the orbital parameters at the CA epoch[16], thereby deriving the distribution of impact points. Subsequently, the asteroid impact probability can be derived by integrating the distribution of impact points within the impact cross-section on the TP.

The isosurface of the distribution function can be used to characterize the distribution contour, where every point on this geometric feature shares an identical probability density value. Fig. 2 presents the isosurface of asteroid 2020 VV's orbit distribution obtained

through the linear approximation method, along with the spatial distribution of MC samples, demonstrating the evolution of orbit distributions at 10, 20, and 50 years after the orbit determination epoch. The plane in the figure is the orbit plane of asteroid 2020 VV, with a heliocentric origin, and the direction x' represents the direction of the ascending node of the orbit on the ecliptic plane. In Cartesian orbital parameters, the velocity is taken as the expectation value of the distribution. The MC samples are obtained through numerical integration, and their distribution can be regarded as the theoretical orbit distribution. Within a relatively short period after the orbit determination epoch (e.g., 10 years), the orbit distribution obtained through the linear approximation method shows high consistency with the theoretical orbit distribution. However, as the duration of orbital dynamical propagation increases, differences between the linear approximation results and the theoretical orbit distribution gradually emerge. After 50 years, the linear approximation results exhibit significant deviations from the theoretical orbit distribution.

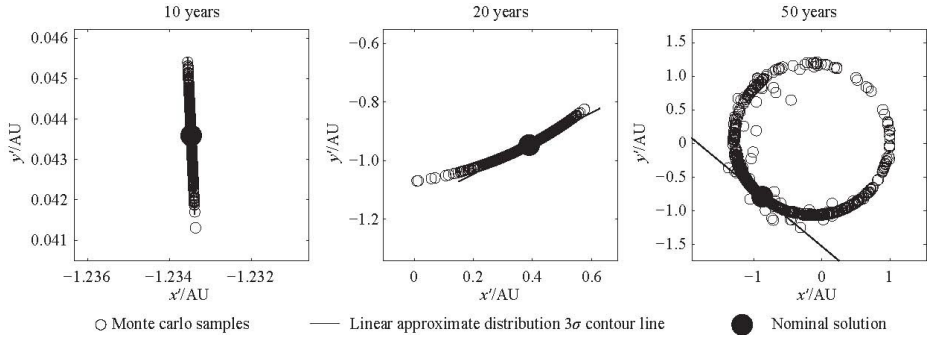

Fig. 2 VAs' coordinate distribution of asteroid 2020 VV in orbit plane.

The LOV impact monitoring system first yields the orbit distribution at the CA epoch through the linear approximation method, and then establishes a linear mapping between the asteroid's impact points on the TP and the orbital parameters at that epoch, which inherently introduces errors. These errors are determined by the geometric feature of the asteroid's orbit distribution and vary among different orbit distributions. The LOV method also introduces another type of errors: During the preliminary search for VIs along the LOV, samples are selected from the LOV itself, and using the LOV as a substitute for CR constitutes an additional approximation. When the asteroid's observational data is relatively sparse, high-precision orbit determination becomes unattainable, and CR becomes wider, resulting in greater errors introduced by using the LOV as a substitute for CR[6].

4. INSTANCES OF IMPACT PROBABILITY ANALYSIS

Six asteroids with the highest cumulative impact probabilities in the NEOCC risk list that

also had warnings in CNEOS (as of June 27, 2023) were selected for impact probability computation. The impact probabilities were computed using the Monte Carlo method described earlier, with the computational process divided into three parts: orbit determination, sampling, orbital dynamical propagation of samples, and impact probability estimation. The orbit computation tool employed in this study was the open-source asteroid orbit computation software OrbFit[1].

The orbit determination was performed using observational data records of these six asteroids obtained from the Minor Planet Center (MPC). The orbital parameter difference indicator δ is defined as:

$$\delta \equiv |\boldsymbol{X}_1 - \boldsymbol{X}_2| = \sqrt{\sum_{i=1}^{6} (X_{1i} - X_{2i})^2}, \tag{10}$$

where $\boldsymbol{X}_1$ and $\boldsymbol{X}_2$ denote orbital parameter vectors. The orbital parameter vectors are nondimensionalized by scaling distances with 1 AU and angles with 1 radian. Table 1 presents the orbit determination results for the six asteroids, along with their difference indicators δ_{MPC} and $\delta_{\mathrm{Horizon}}$ relative to the Minor Planet Center (MPC) and JPL's Horizon system, respectively, where α (semi-major axis), e (eccentricity), i (inclination), Ω (longitude of ascending node), ω (argument of perihelion), and M (mean anomaly) are orbital parameters, and MJD denotes the orbit determination epoch. The orbit determination results showed exceptionally small differences, with the maximum difference indicator δ of the objects on the order of 10^{-3}. Fig. 3 presents the distribution of orbit determination residuals as a function of solar MJD for the six asteroids. All asteroids exhibited orbit determination residuals within a few arcseconds. Through the aforementioned comparison with authoritative solutions and analysis of residual distributions, the orbit determination results were confirmed to be reliable.

Table 1 Orbit determination results for 6 asteroids and difference indicator

Asteroid ID	a/AU	e	$i/^\circ$	$\Omega/^\circ$	$\omega/^\circ$	$M/^\circ$	δ_{MPC}	$\delta_{\mathrm{Horizon}}$	MJD
2020 VW	0.84	0.35	3.04	221.62	41.42	357.09	3.0×10^{-4}	6.7×10^{-4}	60200
2017 WT28	0.90	0.13	5.77	243.06	35.89	114.09	3.4×10^{-3}	5.9×10^{-4}	59000
2006 JY26	1.01	0.08	1.44	43.48	273.67	199.26	1.7×10^{-4}	3.8×10^{-3}	58600
2020 VV	1.12	0.12	0.35	19.65	332.62	74.75	7.6×10^{-6}	7.2×10^{-6}	59200
2020 CQ1	1.44	0.32	2.80	134.35	342.79	41.71	6.5×10^{-5}	6.9×10^{-4}	60200
2022 SX55	0.86	0.40	8.88	354.47	225.16	45.58	9.4×10^{-3}	3.4×10^{-3}	59800

[1]https://adams.dm.unipi.it/~orbmaint/orbfit/

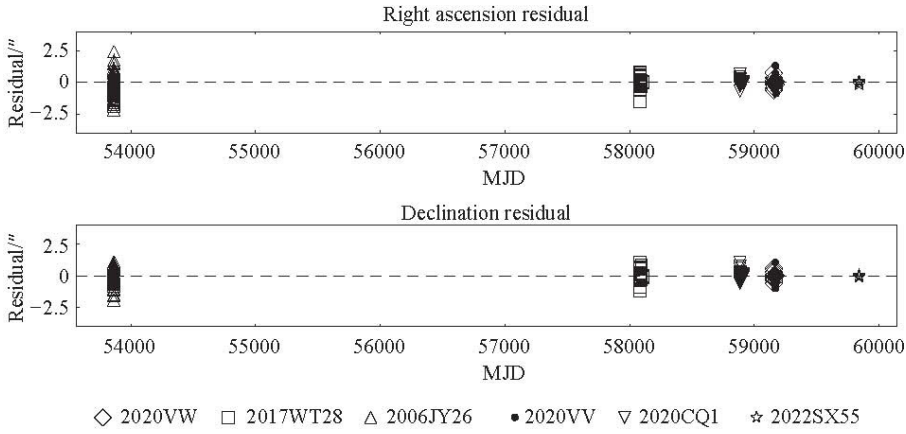

Fig. 3 Orbit determination residuals of six asteroids.

By utilizing orbit determination data, the orbit distribution of the asteroids was obtained, which followed the multivariate Gaussian distribution as given in Eq. (1). VAs were sampled from this distribution, with a sampling size of 10^4 per asteroid. The orbits of VA samples were propagated for 100 years (until January 1, 2124) to assess their Earth-impact probabilities, with impact samples being recorded. The impact probabilities and their uncertainties were computed and then integrated with the warning data of the relevant objects issued by CNEOS and NEOCC, with the final results presented in Table 2, where the "MC" and "Uncertainty" columns respectively denote the impact probabilities and their uncertainties computed in this study, while the "CNEOS" and "NEOCC" columns list the corresponding impact probabilities from two existing impact monitoring systems. The tripartite comparison revealed close agreement between the results of this study and CNEOS results for all objects, with asteroid 2006 JY26 showing the maximum difference (2.1 σ). CNEOS employs a variant of the MC method[5], which is essentially still the MC method in nature, therefore the close agreement between CNEOS results and the results of this study is theoretically expected. NEOCC is an LOV impact monitoring system. Compared with the results from the other two systems using the MC method, significant differences were observed for asteroids 2017 WT28 and 2020 VV, while the results for the other objects showed close agreement.

Table 2 Results of 6 asteroid impact probability analysis

Asteroid ID	MC	CNEOS	NEOCC	Uncertainty
2020 VW	0.0065	0.0070	0.0078	0.00080
2017 WT28	0.0140	0.0120	0.0070	0.00117
2006 JY26	0.0067	0.0050	0.0068	0.00082
2020 VV	0.0024	0.0023	0.0052	0.00049
2020 CQ1	0.0047	0.0046	0.0045	0.00068
2022 SX55	0.0036	0.0040	0.0043	0.00060

Asteroid 2020 VV was selected for further detailed analysis, with the sample size increased to 10^5 for re-computation. The computed impact probability was 2.22×10^{-3} with an uncertainty of 1.49×10^{-4}, showing a 0.2 σ difference from the CNEOS result. In order to investigate the impact sample characteristics of asteroid 2020 VV, Fig. 4 presents the distribution of its impact samples as a function of the approaching date, with the x-axis indicating dates and histogram bars binned by month. The figure illustrates that impactable VA samples are present in 37 distinct months, with October 2056 exhibiting the largest number of impact samples.

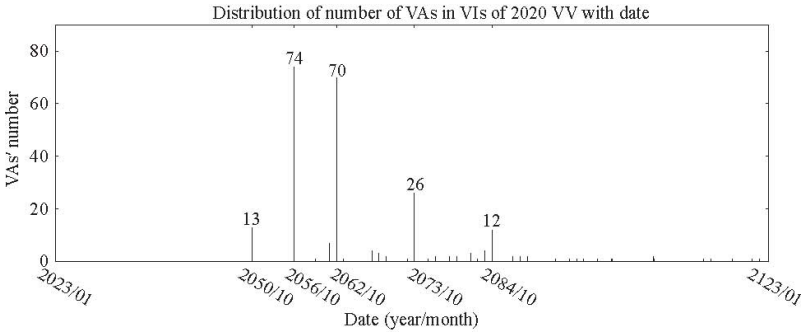

Fig. 4 The number of impactable VAs of asteroid 2020 VV distribution of the frequency of approaching dates.

An analysis was conducted on the impact samples in October 2056. Fig. 5 presents the impact time distribution of asteroid 2020 VV's impact samples in October 2056, with a time span within 3 days and a sample size of 2×10^5. The two vertical dashed lines represent the mean Modified Julian Date (MJD) values of samples in two concentration regions. The temporal distribution is distinctly divided into two regions. The left region has a mean MJD value of 72279.72, while the right region has a mean MJD value of 72282.01. These values correspond to the two predicted impact event warnings in October 2056 as presented in this study. CNEOS also issued two predicted impact event warnings for October 2056, with the MJD values of 72279.65 and 72282.00, respectively. The temporal differences between these

two predicted impact event warnings issued by CNEOS and the results of this study are merely 0.07 days and 0.01 days respectively, indicating excellent agreement with the results as presented in this study.

Theoretically, these two impact events belong to discontinuous VIs in the orbital parameter space, consequently resulting in discontinuous impact outcomes. Fig. 6 presents the TP coordinate system using two mutually perpendicular planes: The left panel shows the TP, while the right panel shows the plane perpendicular to the TP. The coordinate system in the figure displays the orbital coordinates at epoch MJD 72281.99, which is the mean impact epoch value of all impact samples in October 2056. This coordinate system constitutes the TP coordinate system of the nominal orbit, with its origin at the geocenter, where the TP's normal direction s aligns with the nominal orbit's geocentric velocity, while the vertical axis ζ points opposite to the projection of Earth's heliocentric velocity onto the TP, thus $\xi\zeta s$ forming a right-handed system. The $\xi O\zeta$ plane shown in the left panel represents the TP. The figure exhibits three strip-like concentrated distributions of the orbit, each labeled with a serial number, corresponding to three different VIs. According to the definition of the TP, the motion velocity direction of VAs in the figure relative to Earth is approximately perpendicular to the TP. Consequently, these VAs exhibit a significant motion tendency perpendicular to the TP relative to Earth, manifesting as a leftward motion tendency parallel to the plane in the right panel. As time progresses, Earth traverses the three concentrated orbit distributions, resulting in three impact events. However, both this study and CNEOS identified only two VIs. VI 1 occurred first, which exhibited relatively sparse distribution that indicated its relatively lower probability of occurrence, corresponding to the concentration region on the left side of Fig. 5. Subsequently, VI 2 occurred, corresponding to the concentration region on the right side of Fig. 5. However, no impact samples were detected for VI 3.

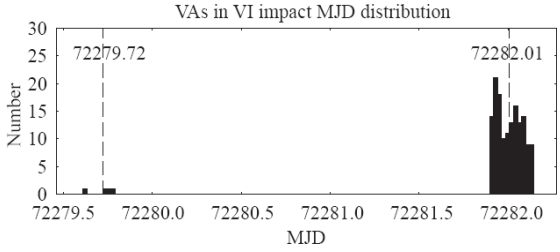

Fig. 5 Impactable VAs' MJD distribution of asteroid 2020 VV of October 2056.

Table 3 Asteroid 2020 VV's VI in October 2056

IM System				
Number	MJD			
	MC	CNEOS	NEOCC	NEODyS
1	72279.72	72279.65	72279.616	72279.640
2	72282.01	72282.00	72281.914	72282.002
3	-	-	72282.003	72282.128

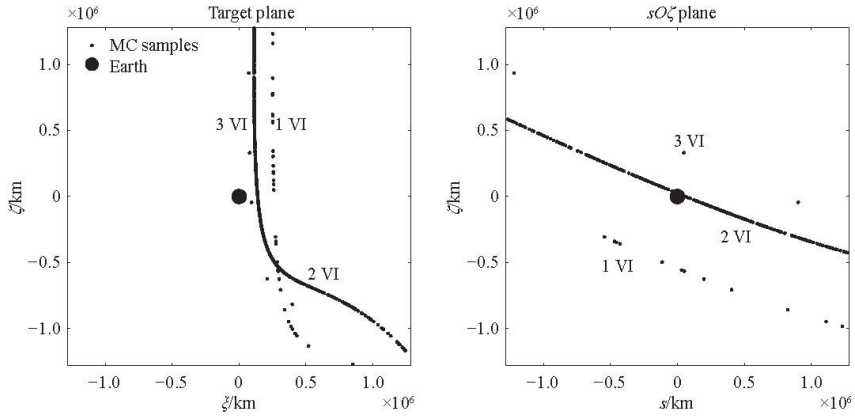

Fig. 6 Distribution of VAs on the target plane coordinate system of asteroid 2020 VV.

Table 3 summarizes the VIs of asteroid 2020 VV in October 2056. Unlike the MC impact monitoring system employed in this study and CNEOS, the two LOV impact monitoring systems, NEOCC and NEODyS, are capable of detecting all three VIs. The LOV impact monitoring system analyzes the CA distance function between LOV samples and Earth, thereby identifying VIs by detecting extremum points of the function[16]. As this process relies on continuous function analysis, it is unaffected by insufficient sampling and thus ensures no VI is missed. In contrast, the MC impact monitoring system may miss VIs with low impact probabilities due to insufficient sampling.

5. CONCLUSIONS

Through analysis of the linear approximation method employed in the LOV impact monitoring system, it was concluded that the deviation between the orbit distribution obtained by this method and the theoretical orbit distribution gradually became significant as the orbit propagation time increased. This study conducted impact analysis on some asteroid instances: Six asteroids with the highest cumulative impact probabilities in the NEOCC risk list that also had warnings in CNEOS (as of June 27, 2023) were selected. The orbital elements of the asteroids were obtained through LS orbit determination, thereby deriving

their orbit distributions. The impact probabilities and their uncertainties were computed using the Monte Carlo method. Compared with CNEOS results, the maximum difference in the impact probabilities of the objects was found to be 2.1 σ. Asteroid 2020 VV was selected for further detailed analysis due to its significant difference in the results of the two types of impact monitoring systems. With a 10-fold increase in sample size, the computed impact probability showed only a 0.2 σ deviation from the CNEOS result. The temporal and spatial distributions of impact samples of asteroid 2020 VV in October 2056 were analyzed, yielding predicted impact event warnings consistent with CNEOS results. Furthermore, it was demonstrated that the LOV impact monitoring system could detect VIs that should theoretically exist but were missed by the MC impact monitoring system. A comparative analysis of the fundamental principles underlying different asteroid impact probability analysis methods revealed: The MC method's substantial demand for computational resources stemmed from its theoretical resolution of computed impact probabilities being inversely proportional to sample size, thereby necessitating extensive sampling and orbit propagation computations to achieve high-resolution estimates; the LOV method required relatively less computational power, as it only involved a relatively small number of orbit propagation computations during the process of searching for VIs. Based on the findings of this study, it can be concluded that the MC impact monitoring system and the LOV impact monitoring system currently have their own advantages and disadvantages: The former avoids errors introduced by the linear approximation method but incurs high computational costs; the latter employs the linear approximation method, which inherently introduces errors, yet it can identify VIs with low impact probabilities that may be missed by the former, while maintaining relatively lower computational costs.

ACKNOWLEDGEMENTS The authors gratefully acknowledge the support from the Cyrus Tang Foundation.

References

1 Li X. R., Zhao H. B., Tang Y. H., et al., Journal of Deep Space Exploration, 2023, 10, 357

2 Milani A., Icarus, 1999, 137, 269

3 Vereš P., Farnocchia D., Chesley S. R., et al., Icarus, 2017, 296, 139

4 Milani A., Chesley S., Chodas P., et al., Asteroid Close Approaches: Analysis and Potential Impact Detection, Asteroids III, 2002

5 Roa J., Farnocchia D., Chesley S. R., ApJ, 2021, 162, 277

6 Tommei G., Universe, 2021, 7, 4

7 Fuentes-Munoz O., Scheeres D. J., Farnocchia D., et al., ApJ, 2023, 166, 10

8 Alessio D., Vigna A. D., CeMDA, 2020, 10, 132

9 Milani A., Gronchi G. F., Knezevic Z., et al., Icarus, 2005, 179, 350

10 Farnocchia D., Chesley S. R., Micheli M., Icarus, 2015, 258, 18

11 Spoto F., Vigna A. D., Milani A., et al., A&A, 2018, 614, A27

12 Solin O., Granvik M., A&A, 2018, 616, A47

13 Milani A., Valsecchi G. B., Icarus, 1999, 140, 408

14 Chodas P. W., Yeomans D. K., ccsl.proc, 1996, 156, 1

15 Rice J. A., Rice J. A., Mathematical Statistics and Data Analysis, Thomson/Brooks/Cole Belmont, CA, 2007, 371

16 Milani A., Chesley S. R., Sansaturio M. E., et al., Icarus, 2005, 173, 362

17 Song Y. Z., Huang Y., Hu X. G., et al., AcASn, 2013, 54, 12

18 Song Y. Z., Huang Y., Hu X. G., et al., ChA&A, 2014, 38, 172